









































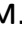
















































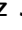
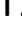




































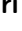






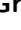



















































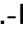
















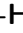
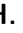






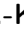







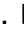


















PREPARED FOR SUBMISSION TO JHEP





# Measurement of branching-fraction ratios and $CP$ asymmetries in $B^\pm \rightarrow D_{CP^\pm} K^\pm$ decays at Belle and Belle II

---

## The Belle and Belle II Collaboration

I. Adachi , L. Aggarwal , H. Aihara , N. Akopov , A. Aloisio , N. Anh Ky ,  
D. M. Asner , H. Atmacan , T. Aushev , V. Aushev , M. Aversano , R. Ayad ,  
V. Babu , H. Bae , S. Bahinipati , P. Bambade , Sw. Banerjee , M. Barrett ,  
J. Baudot , M. Bauer , A. Baur , A. Beaubien , F. Becherer , J. Becker ,  
P. K. Behera , K. Belous , J. V. Bennett , F. U. Bernlochner , V. Bertacchi ,  
M. Bertemes , E. Bertholet , M. Bessner , S. Bettarini , B. Bhuyan ,  
F. Bianchi , T. Bilka , D. Biswas , A. Bobrov , D. Bodrov , A. Bolz ,  
A. Bondar , J. Borah , A. Bozek , M. Bračko , P. Branchini , R. A. Briere ,  
T. E. Browder , A. Budano , S. Bussino , M. Campajola , L. Cao ,  
G. Casarosa , C. Cecchi , J. Cerasoli , M.-C. Chang , P. Chang , P. Cheema ,  
V. Chekelian , B. G. Cheon , K. Chilikin , K. Chirapatpimol , H.-E. Cho ,  
K. Cho , S.-K. Choi , Y. Choi , S. Choudhury , J. Cochran , L. Corona ,  
L. M. Cremaldi , T. Czank , S. Das , F. Dattola , E. De La Cruz-Burelo ,  
S. A. De La Motte , G. de Marino , G. De Nardo , M. De Nuccio ,  
G. De Pietro , R. de Sangro , M. Destefanis , S. Dey , A. De Yta-Hernandez ,  
R. Dhamija , A. Di Canto , F. Di Capua , J. Dingfelder , Z. Doležal ,  
I. Domínguez Jiménez , T. V. Dong , M. Dorigo , K. Dort , D. Dossett ,  
S. Dreyer , S. Dubey , G. Dujany , P. Ecker , M. Eliachevitch , P. Feichtinger ,  
T. Ferber , D. Ferlewicz , T. Fillinger , C. Finck , G. Finocchiaro , A. Fodor ,  
F. Forti , A. Frey , B. G. Fulsom , A. Gabrielli , E. Ganiev ,  
M. Garcia-Hernandez , R. Garg , A. Garmash , G. Gaudino , V. Gaur ,  
A. Gaz , A. Gellrich , G. Ghevondyan , D. Ghosh , H. Ghumaryan ,  
G. Giakoustidis , R. Giordano , A. Giri , B. Gobbo , R. Godang , O. Gogota ,  
P. Goldenzweig , W. Gradl , S. Granderath , E. Graziani , D. Greenwald ,  
Z. Gruberová , T. Gu , Y. Guan , K. Gudkova , S. Halder , Y. Han ,  
T. Hara , K. Hayasaka , H. Hayashii , S. Hazra , C. Hearty , M. T. Hedges ,  
A. Heidelberg , I. Heredia de la Cruz , M. Hernández Villanueva ,  
A. Hershenhorn , T. Higuchi , E. C. Hill , M. Hoek , M. Hohmann , P. Horak ,  
W.-S. Hou , C.-L. Hsu , T. Iijima , K. Inami , N. Ipsita , A. Ishikawa , S. Ito ,  
R. Itoh , M. Iwasaki , P. Jackson , W. W. Jacobs , E.-J. Jang , Q. P. Ji ,  
S. Jia , Y. Jin , A. Johnson , H. Junkerkalefeld , H. Kakuno , A. B. Kaliyar ,  
J. Kandra , K. H. Kang , G. Karyan , T. Kawasaki , F. Keil , C. Ketter 

C. Kiesling , C.-H. Kim , D. Y. Kim , K.-H. Kim , Y.-K. Kim , H. Kindo , K. Kinoshita , P. Kodyš , T. Koga , S. Kohani , K. Kojima , A. Korobov , S. Korpar , E. Kovalenko , R. Kowalewski , T. M. G. Kraetzschmar , P. Križan , P. Krokovny , T. Kuhr , M. Kumar , R. Kumar , K. Kumara , T. Kunigo , A. Kuzmin , Y.-J. Kwon , S. Lacaprara , Y.-T. Lai , T. Lam , L. Lanceri , J. S. Lange , M. Laurenza , R. Leboucher , F. R. Le Diberder , M. J. Lee , P. Leitl , D. Levit , P. M. Lewis , C. Li , J. Li , L. K. Li , Y. Li , J. Libby , Q. Y. Liu , Z. Q. Liu , D. Liventsev , S. Longo , T. Lueck , T. Luo , C. Lyu , Y. Ma , M. Maggiora , S. P. Maharana , R. Maiti , S. Maity , G. Mancinelli , R. Manfredi , E. Manoni , M. Mantovano , D. Marcantonio , S. Marcello , C. Marinas , L. Martel , C. Martellini , A. Martini , T. Martinov , L. Massaccesi , M. Masuda , T. Matsuda , D. Matvienko , S. K. Maurya , J. A. McKenna , R. Mehta , F. Meier , M. Merola , F. Metzner , M. Milesi , C. Miller , M. Mirra , K. Miyabayashi , R. Mizuk , G. B. Mohanty , N. Molina-Gonzalez , S. Mondal , S. Moneta , H.-G. Moser , M. Mrvar , R. Mussa , I. Nakamura , T. Nakano , Y. Nakazawa , A. Narimani Charan , M. Naruki , Z. Natkaniec , A. Natochii , L. Nayak , G. Nazaryan , N. K. Nisar , S. Nishida , S. Ogawa , H. Ono , Y. Onuki , P. Oskin , F. Otani , P. Pakhlov , G. Pakhlova , A. Paladino , A. Panta , E. Paoloni , S. Pardi , K. Parham , H. Park , S.-H. Park , B. Paschen , A. Passeri , S. Patra , S. Paul , T. K. Pedlar , I. Peruzzi , R. Peschke , R. Pestotnik , F. Pham , M. Piccolo , L. E. Piilonen , P. L. M. Podesta-Lerma , T. Podobnik , S. Pokharel , C. Praz , S. Prell , E. Prencipe , M. T. Prim , H. Purwar , N. Rad , P. Rados , G. Raeuber , S. Raiz , M. Reif , S. Reiter , M. Remnev , I. Ripp-Baudot , G. Rizzo , L. B. Rizzuto , S. H. Robertson , M. Roehrken , J. M. Roney , A. Rostomyan , N. Rout , G. Russo , D. Sahoo , S. Sandilya , A. Sangal , L. Santelj , Y. Sato , V. Savinov , B. Scavino , C. Schmitt , G. Schnell , C. Schwanda , A. J. Schwartz , Y. Seino , A. Selce , K. Senyo , J. Serrano , M. E. Sevir , C. Sfienti , W. Shan , C. Sharma , X. D. Shi , T. Shillington , J.-G. Shiu , D. Shtol , A. Sibidanov , F. Simon , J. B. Singh , J. Skorupa , R. J. Sobie , M. Sobotzik , A. Soffer , A. Sokolov , E. Solovieva , S. Spataro , B. Spruck , M. Starič , P. Stavroulakis , S. Stefkova , Z. S. Stottler , R. Stroili , J. Strube , M. Sumihama , K. Sumisawa , W. Sutcliffe , H. Svidras , M. Takahashi , M. Takizawa , U. Tamponi , K. Tanida , F. Tenchini , A. Thaller , O. Tittel , R. Tiwary , D. Tonelli , E. Torassa , N. Toutounji , K. Trabelsi , I. Tsaklidis , M. Uchida , I. Ueda , S. Uehara , Y. Uematsu , T. Uglov , K. Unger , Y. Unno , K. Uno , S. Uno , P. Urquijo , Y. Ushiroda , S. E. Vahsen , R. van Tonder , G. S. Varner , K. E. Varvell , A. Vinokurova , V. S. Vismaya , L. Vitale , V. Vobbiliseti , R. Volpe , B. Wach , M. Wakai , S. Wallner , D. Wang , E. Wang , M.-Z. Wang , Z. Wang , A. Warburton , M. Watanabe , S. Watanuki , M. Welsch , C. Wessel , X. P. Xu , B. D. Yabsley , S. Yamada , W. Yan , S. B. Yang , J. H. Yin , K. Yoshihara , C. Z. Yuan , L. Zani , Y. Zhang 

V. Zhilich , J. S. Zhou , Q. D. Zhou , V. I. Zhukova , R. Žlebčik 

*E-mail:* [coll-publications@belle2.org](mailto:coll-publications@belle2.org)

ABSTRACT:

We report results from a study of  $B^\pm \rightarrow DK^\pm$  decays followed by  $D$  decaying to  $CP$  eigenstates, where  $D$  indicates a  $D^0$  or  $\bar{D}^0$  meson. These decays are sensitive to the Cabibbo-Kobayashi-Maskawa unitarity-triangle angle  $\phi_3$ . The results are based on a combined analysis of the final data set of  $772 \times 10^6$   $B\bar{B}$  pairs collected by the Belle experiment and a data set of  $198 \times 10^6$   $B\bar{B}$  pairs collected by the Belle II experiment, both in electron-positron collisions at the  $\Upsilon(4S)$  resonance. We measure the  $CP$  asymmetries to be  $\mathcal{A}_{CP+} = (+12.5 \pm 5.8 \pm 1.4)\%$  and  $\mathcal{A}_{CP-} = (-16.7 \pm 5.7 \pm 0.6)\%$ , and the ratios of branching fractions to be  $\mathcal{R}_{CP+} = 1.164 \pm 0.081 \pm 0.036$  and  $\mathcal{R}_{CP-} = 1.151 \pm 0.074 \pm 0.019$ . The first contribution to the uncertainties is statistical, and the second is systematic. The asymmetries  $\mathcal{A}_{CP+}$  and  $\mathcal{A}_{CP-}$  have similar magnitudes and opposite signs; their difference corresponds to 3.5 standard deviations. From these values we calculate 68.3% confidence intervals of  $(8.5^\circ < \phi_3 < 16.5^\circ)$  or  $(84.5^\circ < \phi_3 < 95.5^\circ)$  or  $(163.3^\circ < \phi_3 < 171.5^\circ)$  and  $0.321 < r_B < 0.465$ .

KEYWORDS:  $B$  physics,  $CP$ -eigenstates, CKM angle  $\phi_3$  ( $\gamma$ ),  $e^+e^-$  experiments

---

## Contents

<b>1</b>	<b>Introduction</b>	<b>1</b>
<b>2</b>	<b>Data samples and detectors</b>	<b>2</b>
<b>3</b>	<b>Reconstruction and candidate selection</b>	<b>3</b>
<b>4</b>	<b>Fits to data</b>	<b>5</b>
<b>5</b>	<b>Systematic uncertainties</b>	<b>7</b>
<b>6</b>	<b>Results</b>	<b>7</b>
<b>7</b>	<b>Conclusion</b>	<b>9</b>
<b>A</b>	<b>Correlation matrices</b>	<b>16</b>
<b>B</b>	<b><math>D</math> mass sidebands for the <math>B^\pm \rightarrow D_{CP\pm}K^\pm</math> mode</b>	<b>17</b>

---

## 1 Introduction

The Cabibbo-Kobayashi-Maskawa (CKM) matrix parameterizes quark mixing in the standard model [1, 2]. The angle  $\phi_3$ , also called  $\gamma$ , is the phase of a product of its elements  $-V_{ud}V_{ub}^*/V_{cd}^*V_{cb}$ . Theoretical relationships connecting the angle  $\phi_3$  with rates and  $CP$  asymmetries of the decays  $B^\pm \rightarrow DK^\pm$ , where  $D$  indicates a  $D^0$  or  $\bar{D}^0$  meson, are reliable and can be used for precise direct measurements of  $\phi_3$ . Any inconsistency between direct measurements of  $\phi_3$  and the value inferred from global CKM fits performed without this information would show that the CKM mechanism is not a complete description of  $CP$  violation and reveal effects of physics beyond the standard model. Gronau, London, and Wyler (GLW) proposed a method to extract  $\phi_3$  using decays in which the neutral  $D$ ,  $D_{CP\pm}$ , is reconstructed as a  $CP$  eigenstate [3, 4]. We use this method to determine  $\phi_3$  using combined data sets of the Belle and Belle II experiments.

We measure  $CP$  asymmetries,

$$\mathcal{A}_{CP\pm} \equiv \frac{\mathcal{B}(B^- \rightarrow D_{CP\pm}K^-) - \mathcal{B}(B^+ \rightarrow D_{CP\pm}K^+)}{\mathcal{B}(B^- \rightarrow D_{CP\pm}K^-) + \mathcal{B}(B^+ \rightarrow D_{CP\pm}K^+)}, \quad (1.1)$$

and the ratio of branching fractions for decays in which the  $D$  is reconstructed as a  $CP$  eigenstate and decays in which the  $D$  is reconstructed in a flavor-specific state:

$$\mathcal{R}_{CP\pm} \equiv \frac{\mathcal{B}(B^- \rightarrow D_{CP\pm}K^-) + \mathcal{B}(B^+ \rightarrow D_{CP\pm}K^+)}{(\mathcal{B}(B^- \rightarrow D_{\text{flav}}K^-) + \mathcal{B}(B^+ \rightarrow \bar{D}_{\text{flav}}K^+))/2}. \quad (1.2)$$

This ratio can be expressed as

$$\mathcal{R}_{CP\pm} \approx \frac{R_{CP\pm}}{R_{\text{flav}}}, \quad (1.3)$$

where

$$R_{CP\pm} \equiv \frac{\mathcal{B}(B^- \rightarrow D_{CP\pm} K^-) + \mathcal{B}(B^+ \rightarrow D_{CP\pm} K^+)}{\mathcal{B}(B^- \rightarrow D_{CP\pm} \pi^-) + \mathcal{B}(B^+ \rightarrow D_{CP\pm} \pi^+)}, \quad (1.4)$$

and

$$R_{\text{flav}} \equiv \frac{\mathcal{B}(B^- \rightarrow D_{\text{flav}} K^-) + \mathcal{B}(B^+ \rightarrow \bar{D}_{\text{flav}} K^+)}{\mathcal{B}(B^- \rightarrow D_{\text{flav}} \pi^-) + \mathcal{B}(B^+ \rightarrow \bar{D}_{\text{flav}} \pi^+)}. \quad (1.5)$$

In these ratios of branching fractions, most systematic uncertainties, such as those from reconstruction efficiencies and the known  $D$  branching fractions, cancel. The approximation in equation 1.3 is an equality if  $CP$  is conserved in the  $B^\pm \rightarrow D\pi^\pm$  decay. Neglecting the small effects of  $D$  mixing and  $CP$  violation in the  $D^0$  decay [5], we relate  $\mathcal{R}_{CP\pm}$  and  $\mathcal{A}_{CP\pm}$  to  $\phi_3$ , the ratio  $r_B$  of the magnitudes of the suppressed to favored  $B^\pm \rightarrow DK^\pm$  amplitudes, and the relative interaction phase  $\delta_B$  between them [6]:

$$\mathcal{R}_{CP\pm} = 1 + r_B^2 \pm 2r_B \cos \delta_B \cos \phi_3, \quad (1.6)$$

$$\mathcal{A}_{CP\pm} = \pm 2r_B \sin \delta_B \sin \phi_3 / \mathcal{R}_{CP\pm}. \quad (1.7)$$

The current precision on  $\phi_3$  is about  $3.5^\circ$  [6, 7], dominated by recent measurements from the LHCb experiment [8]. The Belle experiment reported a  $\phi_3$ -related measurement using the ADS method [9, 10] for  $B^\pm \rightarrow DK^\pm$  decays with  $D \rightarrow K^\pm \pi^\mp$  using its full data set [11]. A measurement using the BPGGSZ method [12, 13] for  $B^\pm \rightarrow Dh^\pm$  decays with  $D \rightarrow K_s^0 h^\pm h^\mp$ , where  $h$  is a pion or kaon, using the full Belle data set and  $128 \text{ fb}^{-1}$  of data from Belle II was reported recently [14]. However, Belle reported results using the GLW  $B^\pm \rightarrow D^{(*)} K^\pm$  decays based only a fraction of its data [15]. Here we report results based on the full Belle data set and also a fraction of the available data from Belle II. These results supersede those of Ref. [15].

## 2 Data samples and detectors

We analyze samples containing  $772 \times 10^6$  and  $198 \times 10^6$   $B\bar{B}$  pairs collected in electron-positron collisions at the  $\Upsilon(4S)$  resonance with the Belle and Belle II detectors. The integrated luminosities of the corresponding data sets are  $711 \text{ fb}^{-1}$  and  $189 \text{ fb}^{-1}$  for Belle and Belle II. Belle operated at the KEKB asymmetric-energy collider with electron- and positron-beam energies of 8 GeV and 3.5 GeV [16, 17], respectively. Belle II operates at its successor, SuperKEKB, designed to deliver thirty times higher instantaneous luminosity than KEKB, with electron- and positron-beam energies of 7 GeV and 4 GeV [18], respectively.

The Belle detector [19, 20] was a large-solid-angle magnetic spectrometer that consisted of a silicon vertex detector, a 50-layer central drift chamber, an array of aerogel threshold Cherenkov counters, a barrel-like arrangement of time-of-flight scintillation counters, and an electromagnetic calorimeter, all located within a superconducting solenoid coil that

provided a uniform 1.5 T magnetic field collinear with the beams. An iron flux-return yoke located outside the coil was instrumented to detect  $K_L^0$  and muons.

The Belle II detector [21] is an upgrade with several new subdetectors designed to handle the significantly larger beam-related backgrounds of the new collider. It consists of a silicon vertex detector comprising two inner layers of pixel detectors and four outer layers of double-sided silicon strip detectors, a 56-layer central drift chamber, a time-of-propagation detector in the central detector volume and an aerogel ring-imaging Cherenkov detector in the forward region (with respect to the electron-beam’s direction) for charged particle identification (PID), and an electromagnetic calorimeter, all located inside the same solenoid as used for Belle. A flux return outside the solenoid is instrumented with resistive-plate chambers, plastic scintillator modules, and an upgraded read-out system to detect muons,  $K_L^0$  mesons, and neutrons.

We use simulated data to optimize selection criteria, determine detection efficiencies, train multivariate discriminants, identify sources of background, and obtain our fit models. The EVTGEN software package is used to simulate the  $e^+e^- \rightarrow \Upsilon(4S) \rightarrow B\bar{B}$  process and our signal decays [22]. The KKMC [23] and Pythia [24] generators are used to simulate the  $e^+e^- \rightarrow q\bar{q}$  continuum, where  $q$  indicates a  $u, d, s$  or  $c$  quark. For Belle, the GEANT3 package [25] was used to model the detector response, whereas for Belle II the GEANT4 package [26] is used. To account for final-state radiation, the PHOTOS package [27] is used.

### 3 Reconstruction and candidate selection

We use the Belle II analysis software framework to reconstruct both Belle and Belle II data [28–30]. Owing to the different performance of the detectors, separate sets of selection criteria are used for each data set.

Online data-selection criteria are based on requirements of a minimum number of charged particles and observed energy in an event. They are fully efficient for signal and strongly suppress low-multiplicity events. In the offline analysis, reconstructed charged-particle trajectories (tracks) are required to have distances from the  $e^+e^-$  interaction point (IP) smaller than 0.2 cm in the plane transverse to the beams, and smaller than 1.0 cm along the beam direction. Charged kaon and pion candidates are identified based on information from PID detectors and the specific ionisation measured in the drift chamber. We use the ratio  $\mathcal{L}(K/\pi) \equiv \mathcal{L}(K)/[\mathcal{L}(K) + \mathcal{L}(\pi)]$  to identify the type of charged particles, where  $\mathcal{L}(h)$  is the likelihood for a kaon or pion to produce the signals observed in the detectors. Charged particles with  $\mathcal{L}(K/\pi) > 0.6$  are identified as kaons, and those with  $\mathcal{L}(K/\pi) < 0.6$  as pions. To mitigate pion misidentification in the Belle II data, we remove tracks with a polar angle  $\theta > 120^\circ$ , since no PID detector covers this region [31]. No such veto is necessary for Belle data because the larger KEKB boost results in essentially all tracks being within the acceptance of the PID detectors.

We reconstruct  $K_S^0$  candidates in their  $\pi^+\pi^-$  final state by forming each from a pair of oppositely charged particles (assuming they are pions) with a common vertex and mass in the range [486, 509] MeV/ $c^2$  for Belle data and [491, 504] MeV/ $c^2$  for Belle II data. These ranges correspond to  $3\sigma$  in resolution in either direction from the known  $K^0$  mass. To

improve the purity of the  $K_S^0$  sample, we reject combinatorial background using neural networks for Belle data and boosted decision trees for Belle II data [14, 32, 33]. Five input variables are common to the Belle and Belle II discriminators: the angle between the  $K_S^0$  momentum and the direction from the IP to the  $K_S^0$  decay vertex; the distance-of-closest-approach to the IP of the pion tracks; the flight distance of the  $K_S^0$  in the plane transverse to the beams; and the difference between the measured and known  $K_S^0$  masses divided by the uncertainty of the measured mass. The Belle discriminator uses seven additional variables, including the  $K_S^0$  momentum and the shortest distance between the two track helices projected along the beam direction [32, 33]. Each  $K_S^0$  momentum is recalculated from a fit of the pion momenta that constrains them to a common origin.

We reconstruct  $\pi^0$  candidates via their decays to two photons. In Belle data, each photon is required to have an energy above 50 MeV; in Belle II data, each photon is required to have an energy above 80 MeV if detected in the forward endcap, 30 MeV if detected in the barrel, and 60 MeV if in the backward endcap. Each photon must also be unassociated with any track and have an energy-deposition distribution in the calorimeter consistent with an electromagnetic shower. Each  $\pi^0$  candidate must have a mass in the range [120, 145] MeV/ $c^2$ , corresponding to  $2.5\sigma$  in resolution on either side of the known  $\pi^0$  mass, and momentum above 0.6 GeV/ $c$ . Each  $\pi^0$  momentum is recalculated from a fit of the photon momenta that constrains them to a common origin and the diphoton mass to the known mass of the  $\pi^0$ .

A  $D$  candidate is formed from combinations of  $K^-$  and  $\pi^+$ ,  $K^+$  and  $K^-$ , and  $K_S^0$  and  $\pi^0$  candidates. The mass of each  $D$  candidate is required to be consistent with the known  $D$  mass [6] within  $[-20, +20]$  MeV/ $c^2$  in Belle data and  $[-12, +12]$  MeV/ $c^2$  in Belle II data for  $D \rightarrow K^\pm h^\mp$  decays; and within  $[-64, +47]$  MeV/ $c^2$  in Belle data and  $[-53, +36]$  MeV/ $c^2$  in Belle II data for the  $D \rightarrow K_S^0 \pi^0$  decays. These ranges are approximately  $3\sigma$  in resolution on either side of the known mass. Each  $D$  momentum is recalculated from a fit of the momenta of its decay products that constrains them to a common origin and their invariant mass to the known mass of the  $D$  meson.

A  $B$  candidate is formed from a  $D$  candidate and an  $h^\pm$  candidate. To select signal candidates, we use the beam-energy-constrained mass,

$$M_{bc} \equiv c^{-2} \sqrt{E_{\text{beam}}^{*2} - |\vec{p}_B c|^2}, \quad (3.1)$$

and the energy difference,  $\Delta E \equiv E_B - E_{\text{beam}}^*$ , calculated from the  $B$  energy  $E_B$ , momentum  $\vec{p}_B$ , and beam energy  $E_{\text{beam}}^*$ , all in the center-of-mass (c.m.) frame. We require  $M_{bc}$  to be in the range [5.27, 5.29] GeV/ $c^2$ , which is  $\pm 3\sigma$  in resolution around the known  $B$  mass [6]. We require  $\Delta E$  to be in the range  $[-0.13, 0.15]$  GeV to suppress partially reconstructed  $B^\pm \rightarrow D^* h^\pm$  decays, which have negative  $\Delta E$ .

Most remaining backgrounds arise from continuum events, in which final-state particles are highly boosted into two jets that are approximately back-to-back in the c.m. frame. Since  $B\bar{B}$  pairs are produced slightly above kinematic threshold, their final-state particles are isotropically distributed in the c.m. frame. We use boosted decision trees (BDTs) to suppress candidates from continuum events. We train them on equal numbers of simulated

signal and continuum events using variables that are uncorrelated with  $\Delta E$ . Those variables are well simulated, as verified by inspection of the flavor-specific channel. The variables used are modified Fox-Wolfram moments [34, 35]; the cosine of the polar angle of the  $B$  momentum in the c.m. frame; the absolute value of the cosine of the angle between the thrust axis of the  $B$  and the thrust axis of the rest of the charged particles and photons in the event (ROE); the longitudinal distance between the  $B$  vertex and the ROE vertex; and the output of a  $B$ -flavor-tagging algorithm [36, 37]. The thrust axis of a group of particles is the direction that maximizes the sum of the projections of the particle momenta onto it. The BDT classifier output,  $\mathcal{C}$ , is in the range  $[0, 1]$ , peaking at zero for continuum background and at one for signal. We require  $\mathcal{C} > 0.15$ , which retains 95% of signal in Belle data and 97% in Belle II data, while rejecting 60% and 63% of background, respectively.

To suppress  $D$  decays from  $D^* \rightarrow D\pi$  arising from  $e^+e^- \rightarrow c\bar{c} \rightarrow D^*D^{(*)}X$  processes, we use the observed difference between the mass of the  $D$  candidate and the mass of the  $D^*$  candidates reconstructed by associating to the  $D$  any  $\pi^\pm$  or  $\pi^0$  in the ROE. We require that the differences all be outside  $\pm 3\sigma$  in resolution from the known  $D^*-D$  mass difference [6]; the excluded ranges are  $[143.4, 147.5]$  MeV/ $c^2$  and  $[143.8, 147.0]$  MeV/ $c^2$  in Belle and Belle II data for  $D^{*\pm}$ , respectively, and  $[140.0, 145.0]$  MeV/ $c^2$  in both experiments for  $D^{*0}$ . This retains 97% of signal candidates and rejects 13% of background candidates in Belle data and 18% in Belle II data. For  $B^\pm \rightarrow D(\rightarrow K^\pm\pi^\mp)\pi^\pm$ , we require that the dipion mass not be in the range  $[3.08, 3.14]$  GeV/ $c^2$  to veto candidates reconstructed from  $B^\pm \rightarrow J/\psi(\rightarrow \ell^+\ell^-)K^\pm$  decays in which both leptons are misidentified. The  $\Delta E$  distribution of such events peaks in the signal region.

In events with multiple  $B$  candidates, 2% of events for the  $CP$ -even mode and 7% for the  $CP$ -odd mode, we retain the candidate with the smallest  $\chi^2$  calculated from the reconstructed  $D$  mass,  $M_{bc}$  and their resolutions; for decays with  $D_{CP-}$ , the reconstructed  $\pi^0$  mass and its resolution are also used in the  $\chi^2$  calculation. This selects the correct signal candidate in 70%–80% of such events in simulation.

## 4 Fits to data

The final event sample consists of signal, cross-feed background that comes from misidentifying the  $h^\pm$  of a signal event, other  $B\bar{B}$  background sources, and continuum background. To determine the numbers of signal candidates, we fit to the distributions of  $\Delta E$  and  $\mathcal{C}$ , the variables that best discriminate between signal and the remaining background. To make  $\mathcal{C}$  easier to model, we transform it to a new variable  $\mathcal{C}'$ , such that signal is distributed uniformly in  $[0, 1]$  and background is exponentially distributed [38]. We perform an unbinned extended maximum-likelihood fit to candidates with  $\Delta E \in [-0.13, 0.14]$  GeV and  $\mathcal{C}'$  in its full range.

Simulation shows that  $\Delta E$ – $\mathcal{C}'$  correlations in the distributions of candidates from all sample components are negligible, and thus we factorize the two-dimensional probability density function (PDF) for each component in the fit. For each decay mode, we divide the data into 12 subsets defined by the product of the two possible electric charges of the  $B$ , the three possible  $D$  final states (two  $CP$ -specific and one flavor-specific), and whether  $h^\pm$



is identified as a kaon or pion. The fit models are mostly common in all decay modes and data subsets, but the shape parameters are different in each.

For signal, the  $\Delta E$  PDF is the sum of two Gaussian functions and an asymmetric Gaussian function, with all parameters fixed from simulated data except for the common mean of all three  $D$  decay modes and a common multiplier for all signal widths. These parameters are determined by the fit and account for differences in resolution between the experimental and simulated data. The  $\mathcal{C}'$  PDF is a straight line with its slope fixed to the value fitted in the simulated data, except for the PDF used for the Belle  $D\pi$  data, in which the slope is a free parameter.

The cross-feed  $\Delta E$  PDF is same to the signal one, but with its own set of parameters. When determining the fixed parameters of the cross-feed PDF for  $D\pi$ , the simulated data are corrected for momentum-dependent differences in particle misidentification rates between the experimental and simulated data. The  $\mathcal{C}'$  PDF is the sum of a straight line and an exponential function, with parameters fixed from the simulated samples.

For the  $B\bar{B}$  background component, the  $\Delta E$  PDF is the sum of an exponential function and a uniform distribution for the  $CP$  modes, and the sum of an exponential function and a Novosibirsk function [39] for the flavor-specific mode. The  $\mathcal{C}'$  PDF is a straight line whose slope is fixed from simulated data. A peaking background originates from events in which a  $B$  decays directly to  $Xh$  without the production of an intermediate charmed meson in the decay chain. This background is estimated from the  $D$  mass sidebands in data. We find no peaking structure in the sideband of the  $D_{CP-}$  mode, while for the  $D_{CP+}$  mode we see a significant peaking structure and estimate its yield in the signal  $\Delta E$  region to be  $132 \pm 17$  events in Belle data and  $24 \pm 4$  in Belle II data. These yields are estimated by linearly extrapolating the results obtained in eight  $D$  mass sidebands in data, as discussed in Appendix B. In the final fit, the PDF shape of peaking background is fixed from a simulated sample.

For the continuum component, the  $\Delta E$  PDF is a straight line and the  $\mathcal{C}'$  PDF is the sum of two exponential functions. The larger exponential component has its parameter fixed to the value fit from simulated data, and the other free to vary, which accounts for differences between the distributions in experimental and simulated data.

We perform a simultaneous fit to all decay modes in both the Belle and Belle II data, to determine the six charge asymmetries and three branching-fraction ratios. The yields of  $B^\pm \rightarrow Dh^\pm$  with the  $D$  decaying to the state  $X$  and the charged hadron identified as  $h'^\pm$ , denoted as  $Y_{h'}(B^\pm \rightarrow D_X h^\pm)$ , are related to these physical observables via

$$Y_\pi(B^\pm \rightarrow D_X K^\pm) = \frac{1}{2}[1 \mp \mathcal{A}(B \rightarrow D_X K)] N(B \rightarrow D_X \pi) R_X \delta(1 - \varepsilon_\pm), \quad (4.1)$$

$$Y_K(B^\pm \rightarrow D_X K^\pm) = \frac{1}{2}[1 \mp \mathcal{A}(B \rightarrow D_X K)] N(B \rightarrow D_X \pi) R_X \delta\varepsilon_\pm, \quad (4.2)$$

$$Y_\pi(B^\pm \rightarrow D_X \pi^\pm) = \frac{1}{2}[1 \mp \mathcal{A}(B \rightarrow D_X \pi)] N(B \rightarrow D_X \pi) (1 - \kappa_\pm), \quad (4.3)$$

$$Y_K(B^\pm \rightarrow D_X \pi^\pm) = \frac{1}{2}[1 \mp \mathcal{A}(B \rightarrow D_X \pi)] N(B \rightarrow D_X \pi) \kappa_\pm, \quad (4.4)$$

where  $\mathcal{A}$  is the charge asymmetry,  $N$  is the total number of events regardless of how the charged hadron was identified and of its sign,  $\varepsilon_\pm$  is the efficiency to identify a kaon with  $\pm 1$  charge, and  $\kappa_\pm$  is the rate for misidentifying a pion as a kaon with  $\pm 1$  charge. The

efficiency  $\delta$  for reconstructing  $B^\pm \rightarrow DK^\pm$  relative to that for  $B^\pm \rightarrow D\pi^\pm$  is independent of the  $D$  final state and equals 0.975 in Belle data and 1.000 in Belle II data. We measure PID efficiencies and misidentification rates using control samples. For Belle, we measure  $\kappa_+ = 7.7\%$ ,  $\kappa_- = 8.2\%$ ,  $\varepsilon_+ = 83.4\%$ , and  $\varepsilon_- = 84.3\%$  [40]. For Belle II, we measure  $\kappa_+ = 7.2\%$ ,  $\kappa_- = 8.7\%$ ,  $\varepsilon_+ = 79.6\%$ , and  $\varepsilon_- = 78.9\%$ . Uncertainties on those values are typically 0.5%.

The signal yields  $N$  are independent for the Belle and Belle II data. For each background component, separate yields are fitted for  $B^+$  and  $B^-$  to account for their possible charge asymmetries.

To check for fit biases, we perform the fit on five independent sets of simulated data. We also repeat the analysis on 1000 data sets simulated according to the fit model for seven different values of  $\mathcal{A}_{CP^\pm}$ : 0,  $\pm 0.1$ ,  $\pm 0.2$ ,  $\pm 0.3$ . In all cases, the fit results are consistent with the input values.

## 5 Systematic uncertainties

We consider several sources of systematic uncertainties, which are summarized in Table 1. In general, for parameters fixed in the fits, we repeat the fits with the parameter varied by its uncertainty and take the resulting change in our results as the fit-model systematic uncertainty. We do this for the fixed PDF parameters, PID efficiencies and mis-identification rates, peaking background yields, and the efficiency ratio. We ignore correlations between those uncertainties and combine them by adding them in quadrature. We also assign systematic uncertainties (included in the "PDF parameters" item of Table 1) from the difference between correcting and not correcting for the momentum-dependent pion misidentification rates when modeling the cross-feed PDF for the  $D\pi$  data, and having common and independent mode parameters for the  $\Delta E$  PDF's for  $DK$  and  $D\pi$ . We use a common mean for the signal  $\Delta E$  PDFs for all modes. The corresponding systematic uncertainty ("Signal- $\Delta E$  common mean" item of Table 1) is estimated from the variations resulting from assigning different mean values to the  $\Delta E$  PDFs, i.e.,  $B \rightarrow D_X K$  and  $B \rightarrow D_X \pi$  with the same or independent means,  $B^-$  and  $B^+$  with the same or independent means. For the slopes of the  $\mathcal{C}'$  PDF of the  $B\bar{B}$  component, we calculate the systematic uncertainty from the maximum difference among fit results in which the slope is taken from simulation, as in the nominal fit, or taken from the signal  $\mathcal{C}'$  PDF's slope in data, or determined by the fit itself.

## 6 Results

Figures 1, 3, and 5 show distributions and the fit results for candidates satisfying  $|\Delta E| < 0.05$  GeV and  $0.65 < \mathcal{C}' < 1.0$  for Belle data; figures 2, 4, and 6 show the corresponding plots for Belle II data. The fit results agree with the data; the small shifts seen for  $B \rightarrow D_X \pi$  signal in  $\Delta E$  are accounted for in the systematic uncertainty estimation. Table 2 summarizes the signal yields.

**Table 1.** Systematic and statistical uncertainties.

	$\mathcal{R}_{CP+}$	$\mathcal{R}_{CP-}$	$\mathcal{A}_{CP+}$	$\mathcal{A}_{CP-}$
PDF parameters	0.012	0.014	0.002	0.002
PID parameters	0.009	0.010	0.003	0.005
Peaking background yields	0.033	0.002	0.013	—
Efficiency ratio	0.001	0.001	<0.001	<0.001
Signal- $\Delta E$ common mean	0.005	0.006	<0.001	<0.001
Total systematic uncertainty	0.036	0.019	0.014	0.006
Statistical uncertainty	0.081	0.074	0.058	0.057

**Table 2.** Signal yields extracted from the simultaneous fit in data.

$D_X$ mode		$N(B \rightarrow D_X K)$	$N(B \rightarrow D_X \pi)$
$D \rightarrow K^\pm \pi^\mp$	Belle	$4238 \pm 94$	$59481 \pm 267$
	Belle II	$1084 \pm 44$	$14229 \pm 126$
$D \rightarrow K^+ K^-$	Belle	$476 \pm 36$	$5559 \pm 85$
	Belle II	$107 \pm 15$	$1336 \pm 40$
$D \rightarrow K_S^0 \pi^0$	Belle	$541 \pm 42$	$6484 \pm 95$
	Belle II	$145 \pm 16$	$1763 \pm 46$

From the combined Belle and Belle II data, the ratios of branching-fraction ratios and  $CP$  asymmetries of  $B^\pm \rightarrow D_{CP} K^\pm$  are

$$\mathcal{R}_{CP+} = 1.164 \pm 0.081 \pm 0.036, \quad (6.1)$$

$$\mathcal{R}_{CP-} = 1.151 \pm 0.074 \pm 0.019, \quad (6.2)$$

$$\mathcal{A}_{CP+} = (+12.5 \pm 5.8 \pm 1.4)\%, \quad (6.3)$$

$$\mathcal{A}_{CP-} = (-16.7 \pm 5.7 \pm 0.6)\%, \quad (6.4)$$

where the first uncertainty is statistical and the second is systematic.

The significances of  $CP$  violation for  $CP$ -even and  $CP$ -odd  $D$  final states are approximated using  $\sqrt{-2 \ln(\mathcal{L}_0/\mathcal{L}_{\max})} \sigma_{\text{stat}} / \sqrt{\sigma_{\text{stat}}^2 + \sigma_{\text{syst}}^2}$ , where  $\mathcal{L}_{\max}$  is the maximum likelihood value,  $\mathcal{L}_0$  is the likelihood value obtained assuming  $CP$  symmetry, and  $\sigma$  are the statistical and systematic uncertainties. We found  $2.0\sigma$  and  $2.8\sigma$  significances for  $CP$  violation in the  $D_{CP+}$  and  $D_{CP-}$  modes, respectively. This corresponds to  $3.5\sigma$  evidence for the asymmetries being different, i.e.,  $\mathcal{A}_{CP+} \neq \mathcal{A}_{CP-}$ . The measured  $\mathcal{R}_{CP+}$  value is  $2.2\sigma$  away from its expectation as estimated from the world-average values [6, 7] of  $\phi_3$ ,  $r_B$ , and  $\delta_B$ , while the measured  $\mathcal{R}_{CP-}$  value agrees well with its expected value. An underestimation of the peaking-background yield for  $D_{CP+} K$  could be a possible explanation, but this estimation is carefully done using eight different sidebands in data as described in Section 4. Fit bias is also excluded here; we examine data from both realistic simulation and simulation based

**Table 3.** One-dimensional 68.3% and 95.4% CL regions for  $\phi_3$  and  $r_B$ , for  $\phi_3 \in [0^\circ, 180^\circ]$ .

	68.3% CL	95.4% CL
	[8.5, 16.5]	[5.0, 22.0]
$\phi_3$ ( $^\circ$ )	[84.5, 95.5]	[80.0, 100.0]
	[163.3, 171.5]	[157.5, 175.0]
$r_B$	[0.321, 0.465]	[0.241, 0.522]

on the fit model and find no fit bias (Section 4). The  $CP$  asymmetries of  $B^\pm \rightarrow D_X \pi^\pm$  and  $B^\pm \rightarrow D_{\text{flav}} K^\pm$  are  $\mathcal{A}_{CP+}^\pi = (-2.0 \pm 1.4 \pm 0.2)\%$ ,  $\mathcal{A}_{CP-}^\pi = (-0.3 \pm 1.2 \pm 0.2)\%$ ,  $\mathcal{A}_{\text{flav}}^\pi = (-0.5 \pm 0.4 \pm 0.2)\%$ , and  $\mathcal{A}_{\text{flav}}^K = (-1.4 \pm 1.7 \pm 0.1)\%$ , consistent with the expected  $CP$  symmetry in these modes.

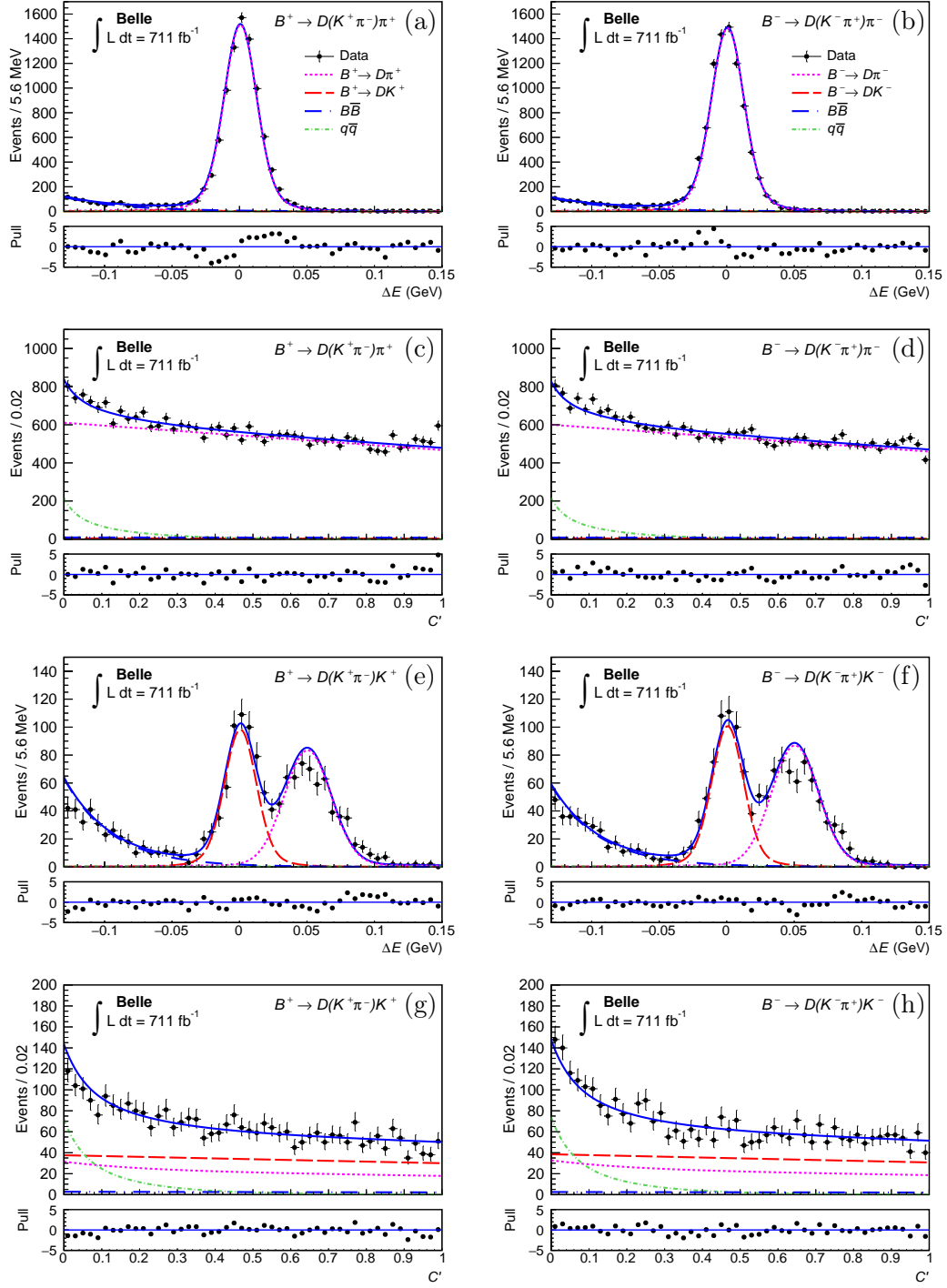
With these results for  $R_{CP\pm}$  and  $\mathcal{A}_{CP\pm}$ , we constrain the angle  $\phi_3$  using a frequentist approach as implemented in the CKMFITTER package [41]. Figure 7 shows the resulting distributions of the  $p$ -value (the complement of the confidence level,  $1 - \text{CL}$ ). Given the  $\delta_B \leftrightarrow \phi_3$  symmetry of equation 1.6 and 1.7, the distribution for  $\delta_B$  is identical to that for  $\phi_3$ . Table 3 lists the 68.3%- and 95.4%-CL intervals for  $\phi_3$  and  $r_B$  for solutions with  $\phi_3 \in [0^\circ, 180^\circ]$ . The large value measured for  $\mathcal{R}_{CP+}$  results in a relatively large  $r_B$  which, in turn, gives a stringent constraint on  $\phi_3$  due to the correlation between  $r_B$  and  $\phi_3$ .

## 7 Conclusion

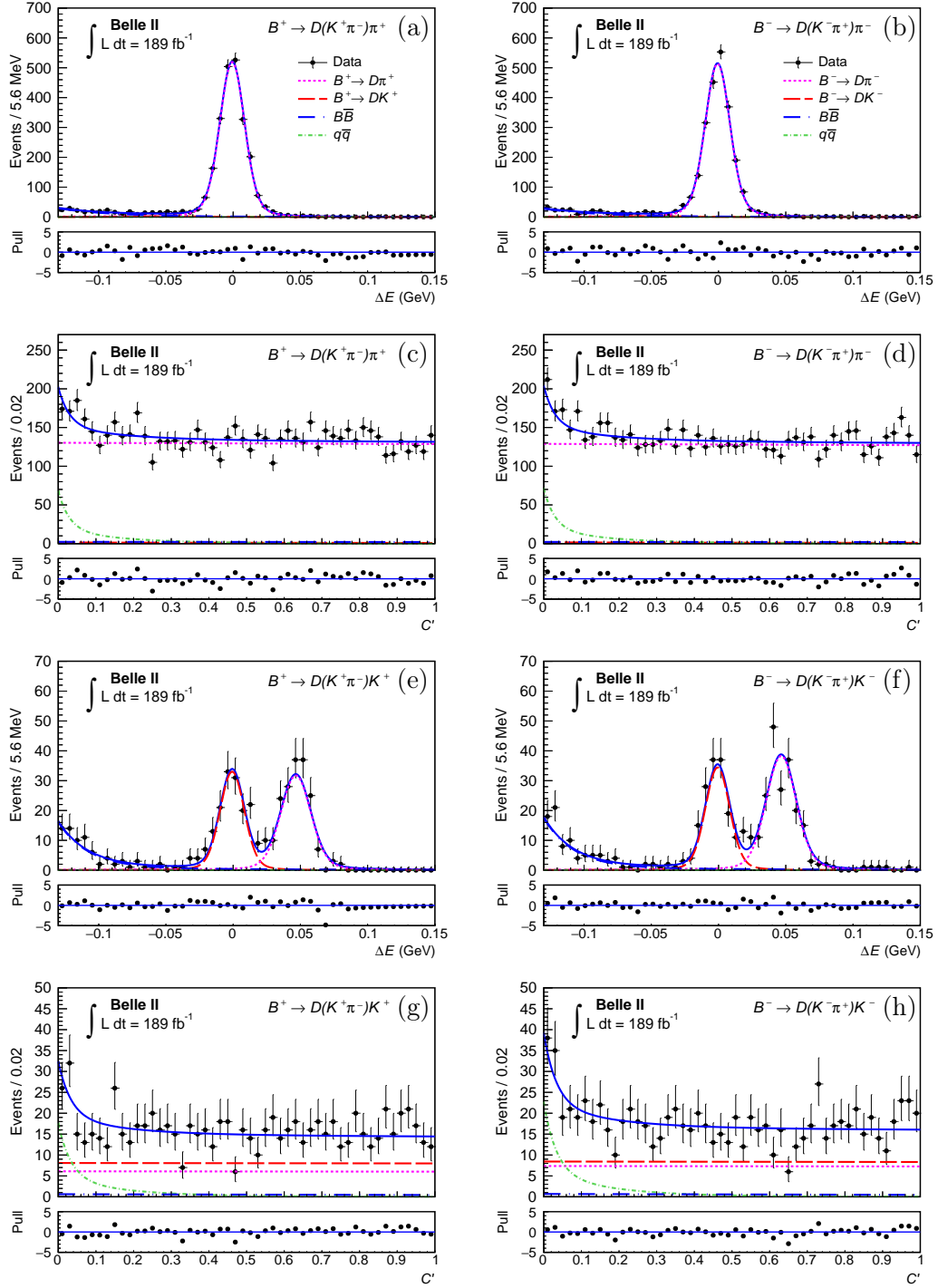
We measure the  $CP$  asymmetries and ratios of branching-fraction ratios for  $B^\pm \rightarrow D_{CP\pm} K^\pm$  for the  $CP$ -odd  $D$  final state  $K^+ K^-$  and the  $CP$ -even final state  $K_S^0 \pi^0$  with a combined analysis of the full Belle data set of  $772 \times 10^6$   $B\bar{B}$  pairs and a Belle II data set containing  $198 \times 10^6$   $B\bar{B}$  pairs. As expected, the asymmetries have opposite signs, showing prominent  $CP$  violation in  $B^\pm \rightarrow D_{CP} K^\pm$ . The statistical and systematic precision of our results, based on a data set almost four times larger than the previous Belle measurement [15], is significantly improved. The results are consistent with those of the BABAR and LHCb experiments [42, 43]. We obtain 68.3%-CL intervals for the CKM angle  $\phi_3$  and the amplitude ratio  $r_B$ :

$$\phi_3 \in [8.5^\circ, 16.5^\circ] \cup [84.5^\circ, 95.5^\circ] \cup [163.3^\circ, 171.5^\circ], \quad (7.1)$$

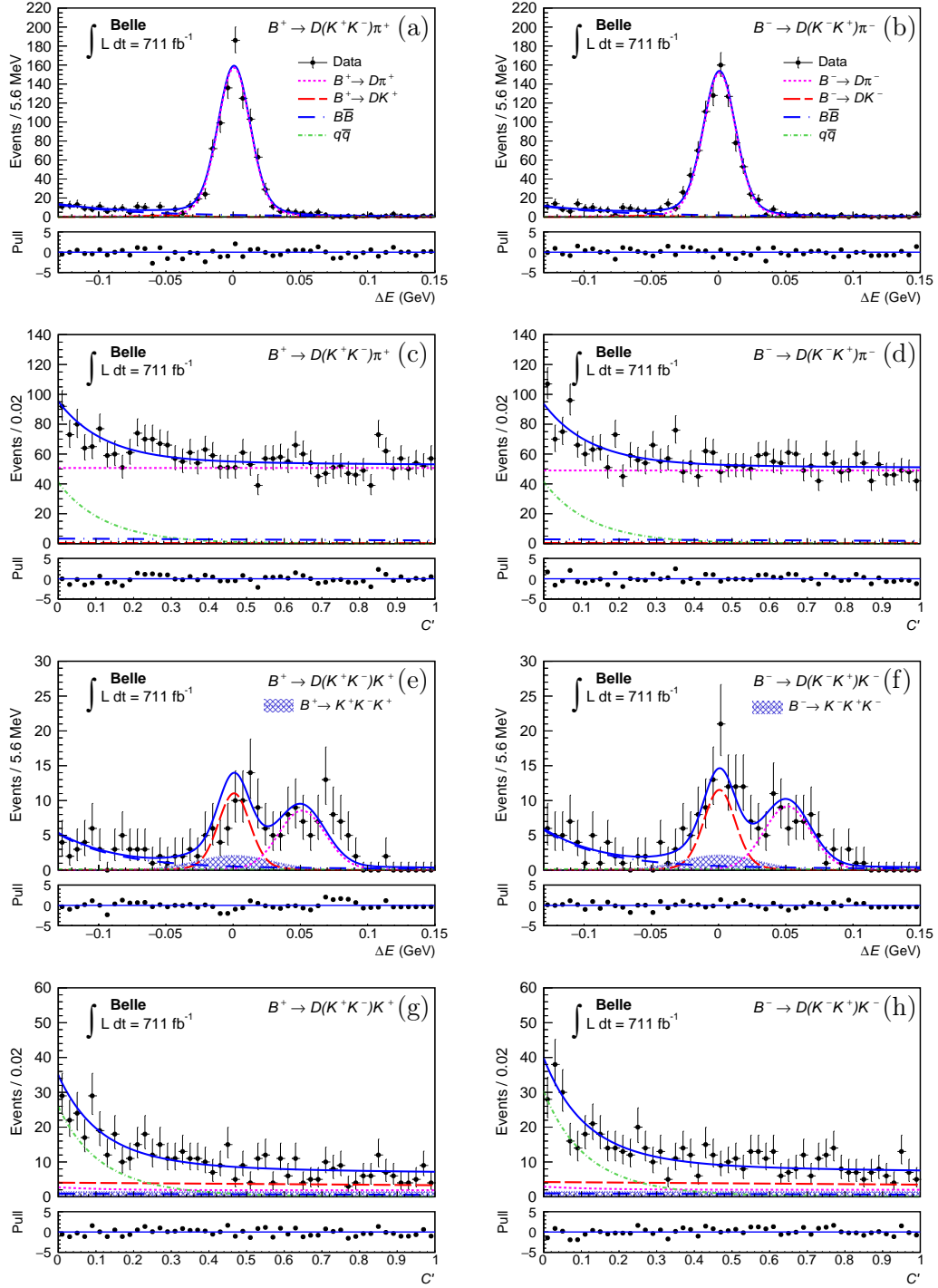
$$r_B \in [0.321, 0.465]. \quad (7.2)$$



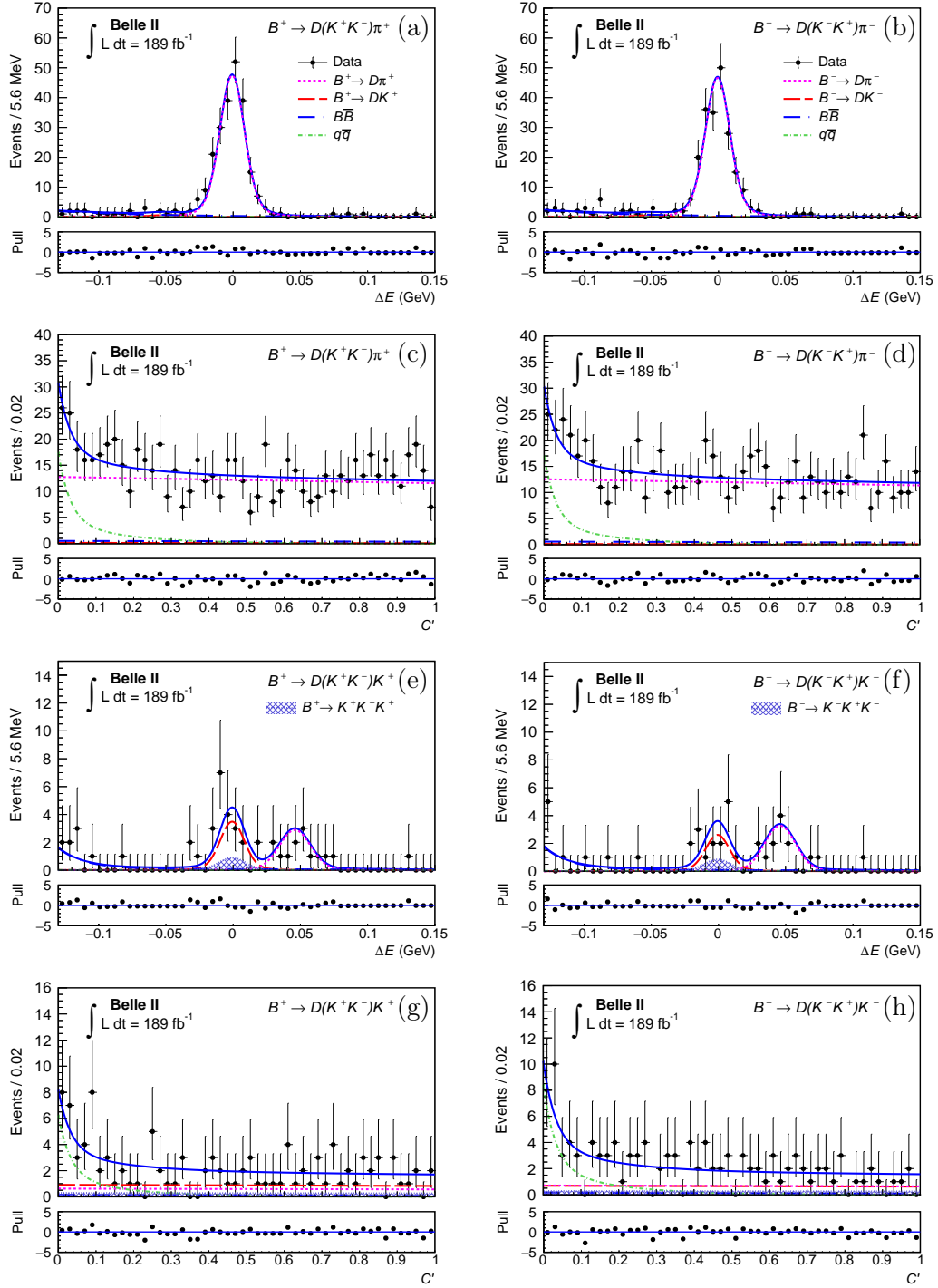
**Figure 1.** Distributions of  $\Delta E$  and  $C'$  for  $B^\pm \rightarrow D(\rightarrow K^\pm \pi^\mp) h^\pm$  candidates in the Belle data with fit projections overlaid. Differences between data and fit results normalized by the uncertainty in data are shown in the bottom panels.



**Figure 2.** Distributions of  $\Delta E$  and  $C'$  for  $B^\pm \rightarrow D(\rightarrow K^\pm\pi^\mp)h^\pm$  candidates in the Belle II data with fit projections overlaid. Differences between data and fit results normalized by the uncertainty in data are shown in the bottom panels.

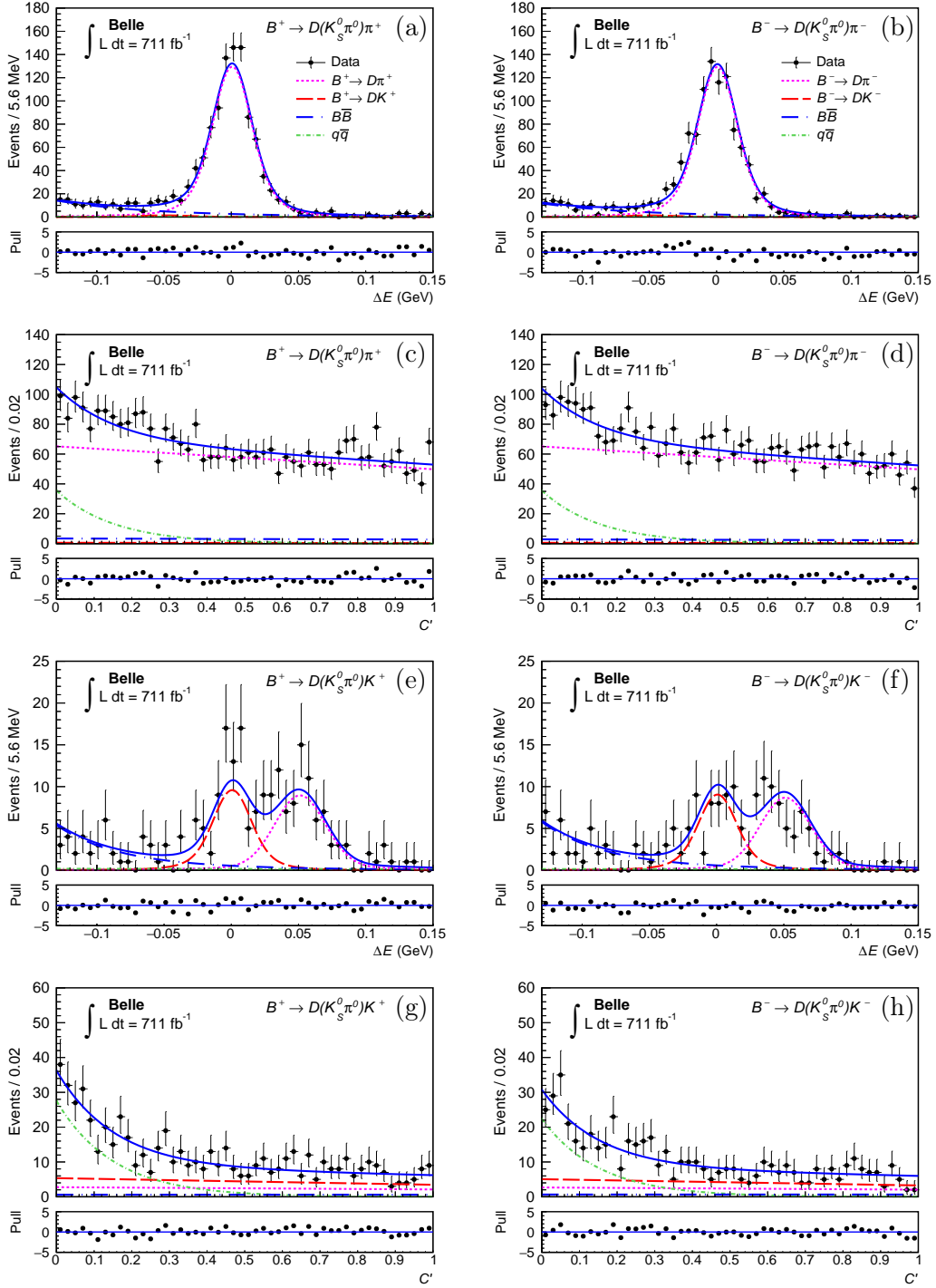


**Figure 3.** Distributions of  $\Delta E$  and  $C'$  for  $B^\pm \rightarrow D(\rightarrow K^+K^-)h^\pm$  candidates in the Belle data with fit projections overlaid. Differences between data and fit results normalized by the uncertainty in data are shown in the bottom panels.

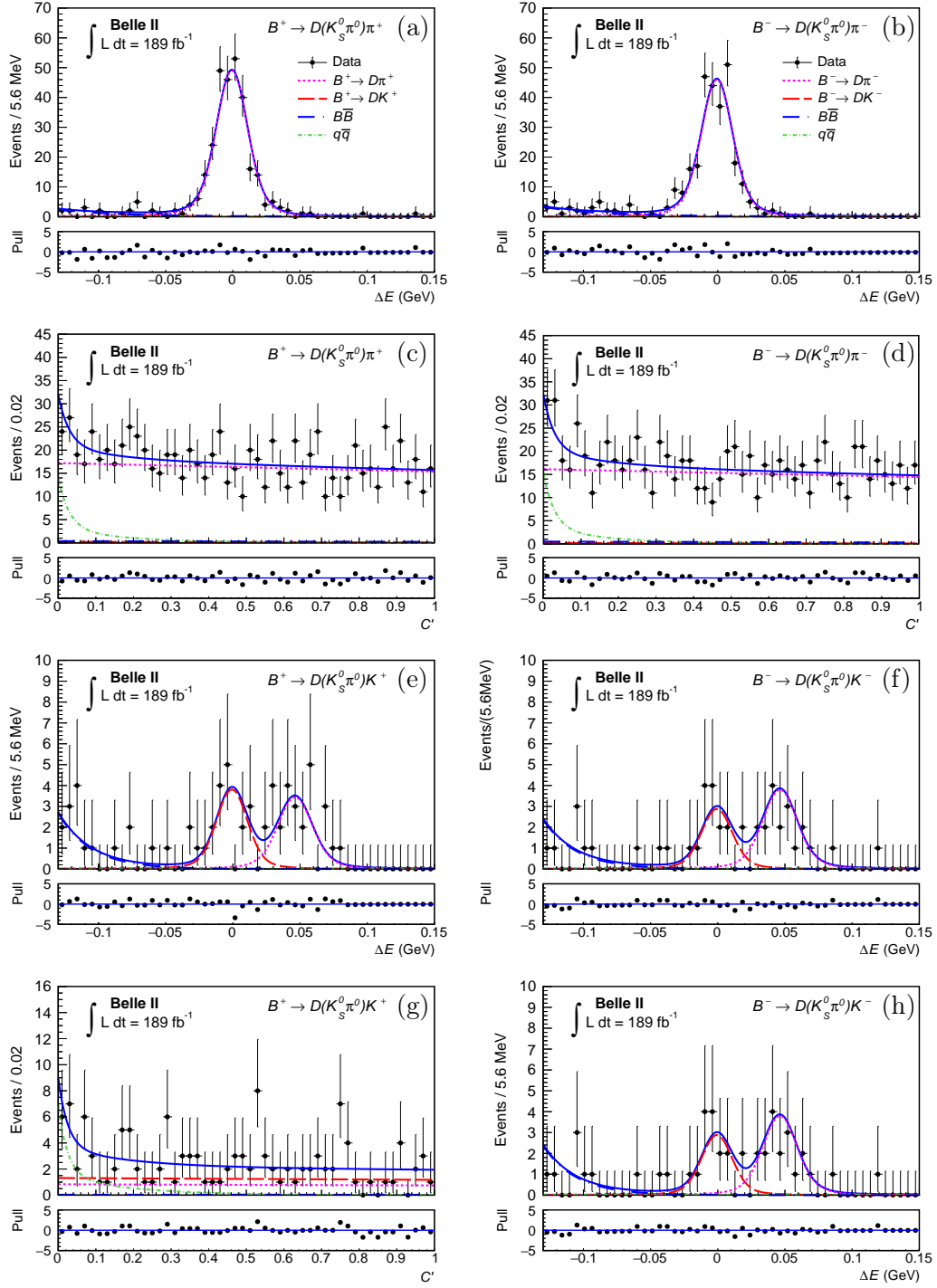


**Figure 4.** Distributions of  $\Delta E$  and  $C'$  for  $B^\pm \rightarrow D(\rightarrow K^+K^-)h^\pm$  candidates in the Belle II data with fit projections overlaid. Differences between data and fit results normalized by the uncertainty in data are shown in the bottom panels.

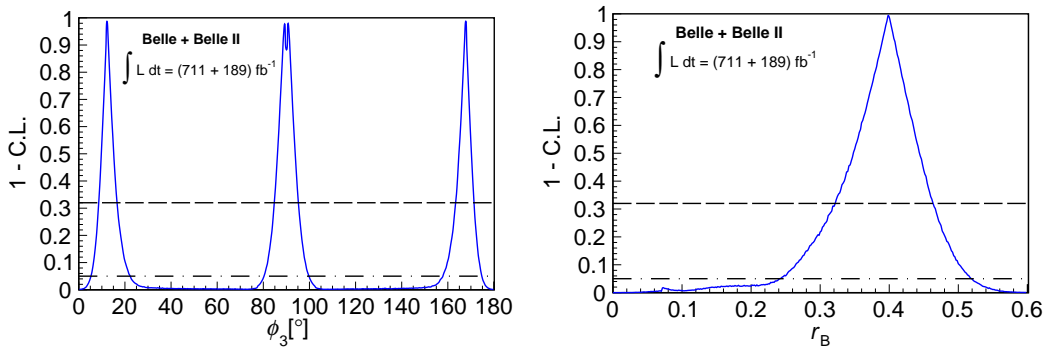




**Figure 5.** Distributions of  $\Delta E$  and  $C'$  for  $B^\pm \rightarrow D(\rightarrow K_s^0 \pi^0)h^\pm$  candidates in the Belle data with fit projections overlaid. Differences between data and fit results normalized by the uncertainty in data are shown in the bottom panels.



**Figure 6.** Distributions of  $\Delta E$  and  $C'$  for  $B^\pm \rightarrow D(\rightarrow K_S^0 \pi^0)h^\pm$  candidates in the Belle II data with fit projections overlaid. Differences between data and fit results normalized by the uncertainty in data are shown in the bottom panels.



**Figure 7.**  $p$ -values ( $1 - \text{CL}$ ) as functions of  $\phi_3$  (left) and  $r_B$  (right). The dashed horizontal line shows the 68.3% CL, and the dash-dotted line shows the 95.4% CL.

## A Correlation matrices

Table 4 and 5 list the statistical and systematic correlation matrices for  $\mathcal{A}_{CP\pm}$  and  $\mathcal{R}_{CP\pm}$ . We vary every fixed parameter randomly by Gaussian distribution for thousand times. We repeat the fit with the varied values for every fixed parameter, which can result in Gaussian-like distributions of the measured observables. The correlations are calculated by using those Gaussian-like distributions. These correlation matrices are used in the extraction of  $\phi_3$ ,  $\delta_B$  and  $r_B$ .

**Table 4.** Statistical correlation matrix of measured observables.

	$\mathcal{R}_{CP+}$	$\mathcal{R}_{CP-}$	$\mathcal{A}_{CP+}$	$\mathcal{A}_{CP-}$
$\mathcal{R}_{CP+}$	1	-0.081	0.060	0.000
$\mathcal{R}_{CP-}$		1	0.000	0.056
$\mathcal{A}_{CP+}$			1	0.000
$\mathcal{A}_{CP-}$				1

**Table 5.** Systematic correlation matrix of measured observables.

	$\mathcal{R}_{CP+}$	$\mathcal{R}_{CP-}$	$\mathcal{A}_{CP+}$	$\mathcal{A}_{CP-}$
$\mathcal{R}_{CP+}$	1	-0.063	0.342	0.005
$\mathcal{R}_{CP-}$		1	-0.128	-0.490
$\mathcal{A}_{CP+}$			1	0.542
$\mathcal{A}_{CP-}$				1

## B $D$ mass sidebands for the $B^\pm \rightarrow D_{CP^+}K^\pm$ mode

In Section 4, we use eight  $D$  mass sidebands of data to estimate the peaking background for the  $D_{CP^+}$  mode. Table 6 lists the sideband mass ranges used in the Belle and Belle II analyses, respectively. These sidebands are chosen to extend over the same range as the signal  $D$  region.

**Table 6.**  $D$  sideband mass regions for  $D_{CP^+}$  mode, in  $\text{GeV}/c^2$  units.

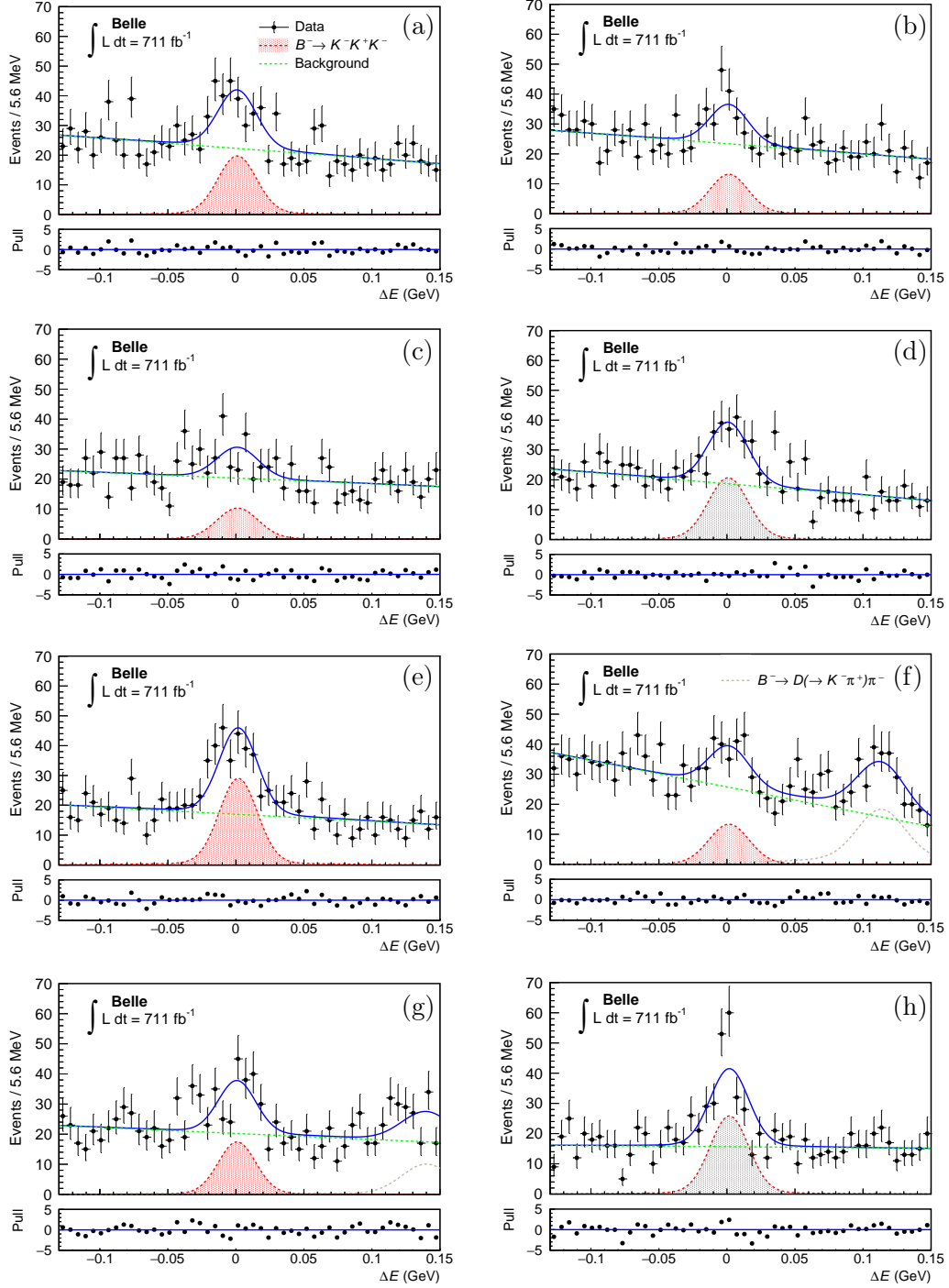
Analysis	Lower sidebands	Upper sidebands
Belle	[1.67,1.71][1.71,1.75]	[1.90,1.94][1.94,1.98]
	[1.75,1.79][1.79,1.83]	[1.98,2.02][2.02,2.06]
Belle II	[1.706,1.732][1.732,1.758]	[1.758,1.784][1.784,1.810]
	[1.920,1.946][1.946,1.972]	[1.972,1.998][1.998,2.024]

Fig 8 shows distributions and fit-result projections in the data sidebands for the Belle analysis. We obtain the peaking background yield for each sideband and interpolate those yields linearly.

The Belle II data sample used in this analysis has only an integrated luminosity of  $189 \text{ fb}^{-1}$ , which is insufficient to estimate the yield of peaking background. Instead we obtain the Belle II yield by scaling the Belle yield by the reconstruction efficiencies  $\epsilon$  of  $B^- \rightarrow K^-K^+K^-$  in simulated data and the luminosities ( $L$ ) of Belle and Belle II data samples:

$$Y_{B2}(B^- \rightarrow K^-K^+K^-) = Y_B(B^- \rightarrow K^-K^+K^-) \frac{\epsilon_{B2}L_{B2}}{\epsilon_B L_B}, \quad (\text{B.1})$$

where subscripts  $B$  and  $B2$  stand for Belle and Belle II, respectively.



**Figure 8.**  $\Delta E$  distributions of  $B^\pm \rightarrow D(\rightarrow K^-K^+)K^\pm$  in Belle data with the fit projections overlaid for the lower sidebands [1.67, 1.71]  $\text{GeV}/c^2$  (a), [1.71, 1.75]  $\text{GeV}/c^2$  (b), [1.75, 1.79]  $\text{GeV}/c^2$  (c), and [1.79, 1.83]  $\text{GeV}/c^2$  (d), and the upper sidebands [1.90, 1.94]  $\text{GeV}/c^2$  (e), [1.94, 1.98]  $\text{GeV}/c^2$  (f), [1.98, 2.02]  $\text{GeV}/c^2$  (g), and [2.02, 2.06]  $\text{GeV}/c^2$  (h).

## Acknowledgments

This work, based on data collected using the Belle II detector, which was built and commissioned prior to March 2019, was supported by Science Committee of the Republic of Armenia Grant No. 20TTTCG-1C010; Australian Research Council and Research Grants No. DP200101792, No. DP210101900, No. DP210102831, No. DE220100462, No. LE210100098, and No. LE230100085; Austrian Federal Ministry of Education, Science and Research, Austrian Science Fund No. P 31361-N36 and No. J4625-N, and Horizon 2020 ERC Starting Grant No. 947006 “InterLeptons”; Natural Sciences and Engineering Research Council of Canada, Compute Canada and CANARIE; National Key R&D Program of China under Contract No. 2022YFA1601903, National Natural Science Foundation of China and Research Grants No. 11575017, No. 11761141009, No. 11705209, No. 11975076, No. 12135005, No. 12150004, No. 12161141008, and No. 12175041, and Shandong Provincial Natural Science Foundation Project ZR2022JQ02; the Czech Science Foundation Grant No. 22-18469S; European Research Council, Seventh Framework PIEF-GA-2013-622527, Horizon 2020 ERC-Advanced Grants No. 267104 and No. 884719, Horizon 2020 ERC-Consolidator Grant No. 819127, Horizon 2020 Marie Skłodowska-Curie Grant Agreement No. 700525 “NIOBE” and No. 101026516, and Horizon 2020 Marie Skłodowska-Curie RISE project JENNIFER2 Grant Agreement No. 822070 (European grants); L’Institut National de Physique Nucléaire et de Physique des Particules (IN2P3) du CNRS and L’Agence Nationale de la Recherche (ANR) under grant ANR-21-CE31-0009 (France); BMBF, DFG, HGF, MPG, and AvH Foundation (Germany); Department of Atomic Energy under Project Identification No. RTI 4002 and Department of Science and Technology (India); Israel Science Foundation Grant No. 2476/17, U.S.-Israel Binational Science Foundation Grant No. 2016113, and Israel Ministry of Science Grant No. 3-16543; Istituto Nazionale di Fisica Nucleare and the Research Grants BELLE2; Japan Society for the Promotion of Science, Grant-in-Aid for Scientific Research Grants No. 16H03968, No. 16H03993, No. 16H06492, No. 16K05323, No. 17H01133, No. 17H05405, No. 18K03621, No. 18H03710, No. 18H05226, No. 19H00682, No. 22H00144, No. 22K14056, No. 23H05433, No. 26220706, and No. 26400255, the National Institute of Informatics, and Science Information NETwork 5 (SINET5), and the Ministry of Education, Culture, Sports, Science, and Technology (MEXT) of Japan; National Research Foundation (NRF) of Korea Grants No. 2016R1D1A1B02012900, No. 2018R1A2B-3003643, No. 2018R1A6A1A06024970, No. 2019R1I1A3A01058933, No. 2021R1A6A1A-03043957, No. 2021R1F1A1060423, No. 2021R1F1A1064008, No. 2022R1A2C1003993, and No. RS-2022-00197659, Radiation Science Research Institute, Foreign Large-size Research Facility Application Supporting project, the Global Science Experimental Data Hub Center of the Korea Institute of Science and Technology Information and KREONET/GLORIAD; Universiti Malaya RU grant, Akademi Sains Malaysia, and Ministry of Education Malaysia; Frontiers of Science Program Contracts No. FOINS-296, No. CB-221329, No. CB-236394, No. CB-254409, and No. CB-180023, and SEP-CINVESTAV Research Grant No. 237 (Mexico); the Polish Ministry of Science and Higher Education and the National Science Center; the Ministry of Science and Higher Education of the Russian Federation, Agreement No. 14.W03.31.0026, and the HSE University Basic Research Program, Moscow; University

of Tabuk Research Grants No. S-0256-1438 and No. S-0280-1439 (Saudi Arabia); Slovenian Research Agency and Research Grants No. J1-9124 and No. P1-0135; Agencia Estatal de Investigacion, Spain Grant No. RYC2020-029875-I and Generalitat Valenciana, Spain Grant No. CIDEGENT/2018/020 Ministry of Science and Technology and Research Grants No. MOST106-2112-M-002-005-MY3 and No. MOST107-2119-M-002-035-MY3, and the Ministry of Education (Taiwan); Thailand Center of Excellence in Physics; TUBITAK ULAKBIM (Turkey); National Research Foundation of Ukraine, Project No. 2020.02/0257, and Ministry of Education and Science of Ukraine; the U.S. National Science Foundation and Research Grants No. PHY-1913789 and No. PHY-2111604, and the U.S. Department of Energy and Research Awards No. DE-AC06-76RLO1830, No. DE-SC0007983, No. DE-SC0009824, No. DE-SC0009973, No. DE-SC0010007, No. DE-SC0010073, No. DE-SC0010118, No. DE-SC0010504, No. DE-SC0011784, No. DE-SC0012704, No. DE-SC0019230, No. DE-SC0021274, No. DE-SC0022350, No. DE-SC0023470; and the Vietnam Academy of Science and Technology (VAST) under Grant No. DL0000.05/21-23.

These acknowledgements are not to be interpreted as an endorsement of any statement made by any of our institutes, funding agencies, governments, or their representatives.

We thank the SuperKEKB team for delivering high-luminosity collisions; the KEK cryogenics group for the efficient operation of the detector solenoid magnet; the KEK computer group and the NII for on-site computing support and SINET6 network support; and the raw-data centers at BNL, DESY, GridKa, IN2P3, INFN, and the University of Victoria for offsite computing support.

## References

- [1] N. Cabibbo, *Unitary Symmetry and Leptonic Decays*, *Phys. Rev. Lett.* **10**, 531 (1963) .
- [2] M. Kobayashi and T. Maskawa, *CP violation in the renormalizable theory of weak interaction*, *Prog. Theor. Phys.* **49**, 652 (1973).
- [3] M. Gronau and D. London, *How to determine all the angles of the unitarity triangle from  $B_d^0 \rightarrow DK_S$  and  $B_s^0 \rightarrow D\varphi$*  , *Phys. Lett. B* **253**, 483 (1991) .
- [4] M. Gronau and D. Wyler, *On determining a weak phase from charged B decay asymmetries*, *Phys. Lett. B* **265**, 172 (1991).
- [5] M. Rama, *Effect of  $D$ - $\bar{D}$  mixing in the extraction of  $\gamma$  with  $B^- \rightarrow D^0 K^-$  and  $B^- \rightarrow D^0 \pi^-$  decays*, *Phys. Rev. D* **89**, 014021 (2014).
- [6] R. L. Workman *et al.* (PARTICLE DATA GROUP), *Review of Particle Physics*, *Prog. Theor. Exp. Phys.* **2022**, 083C01 (2022) and 2023 update.
- [7] Y. Amhis *et al.* (HEAVY FLAVOR AVERAGING GROUP collaboration), *Averages of b-hadron, c-hadron, and  $\tau$ -lepton properties as of 2021*, *Phys. Rev. D* **107**, 052008 (2023).
- [8] R. Aaij *et al.*, LHCb collaboration, *Simultaneous determination of the CKM angle  $\gamma$  and parameters related to mixing and CP violation in the charm sector*, LHCb-CONF-2022-003.
- [9] D. Atwood, I. Dunietz, and A. Soni, *Enhanced CP violation with  $B \rightarrow KD^0(\bar{D}^0)$  modes and extraction of the CKM angle  $\gamma$* , *Phys. Rev. Lett.* **78**, 3257 (1997).
- [10] D. Atwood, I. Dunietz, and A. Soni, *Improved methods for observing CP violation in  $B^\pm \rightarrow K^\pm D$  and measuring the CKM phase  $\gamma$* , *Phys. Rev. D* **63**, 036005 (2001).
- [11] Y. Horii *et al.*, BELLE collaboration, *Evidence for the Suppressed Decay  $B^- \rightarrow DK^-$ ,  $D \rightarrow K^+ \pi^-$* , *Phys. Rev. Lett.* **106**, 231803 (2011).
- [12] A. Giri, Y. Grossman, A. Soffer, and J. Zupan, *Determining  $\gamma$  using  $B^\pm \rightarrow DK^\pm$  with multibody D decays*, *Phys. Rev. D* **68**, 054018 (2003).
- [13] A. Bondar, *Proceedings of BINP Special Analysis Meeting on Dalitz Analysis*, (unpublished) 2002.
- [14] F. Abudinen *et al.*, BELLE and BELLE II collaborations, *Combined analysis of Belle and Belle II data to determine the CKM angle  $\phi_3$  using  $B^+ \rightarrow D(K_S^0 h^+ h^-)h^+$  decays*, *J. High Energy Phys.* **63** (2022).
- [15] K. Abe *et al.*, BELLE collaboration, *Study of  $B^\pm \rightarrow D_{CP^\pm} K^\pm$  and  $D_{CP^\pm}^* K^\pm$  decays*, *Phys. Rev. D* **73**, 051106 (2006).
- [16] S. Kurokawa and E. Kikutani, *Overview of the KEKB accelerators*, *Nucl. Instrum. Meth. A* **499**, 1 (2003).
- [17] T. Abe *et al.*, *Achievement of the KEKB*, *Prog. Theor. Exp. Phys.* (2013) 03A001-03A011.
- [18] K. Akai, K. Furukawa, and H. Koiso, *SuperKEKB Collider*, *Nucl. Instrum. Meth. A* **907** (2018) 188.
- [19] A. Abashian *et al.*, BELLE collaboration, *The Belle Detector*, *Nucl. Instrum. Meth. A* **479**, (2002) 117.
- [20] J. Brodzicka *et al.*, *Physics Achievements from the Belle Experiment*, *Prog. Theor. Exp. Phys.* (2012) 04D001.



- [21] T. Abe *et al.*, BELLE II collaboration, *Belle II Technical Design Report*, [[arXiv:1101.0352](https://arxiv.org/abs/1101.0352)].
- [22] D. J. Lange, *The EVTGEN particle decay simulation package*, *Nucl. Instrum. Meth. A* **462**, (2001) 152.
- [23] B. Ward, S. Jadach and Z. Was, *Precision calculation for  $e^+e^- \rightarrow 2f$ : The KK MC project*, *Nucl. Phys. B Proc. Suppl.* **116** (2003) 73.
- [24] T. Sjöstrand *et al.*, *A Brief Introduction to PYTHIA 8.1*, *Comput. Phys. Commun.* **178** (2008) 852.
- [25] R. Brun *et al.*, *GEANT 3.21*, CERN-DD-EE-84-01 (1984) [[INSPIRE](https://arxiv.org/abs/1905.09017)].
- [26] S. Agostinelli *et al.*, *GEANT4 - a simulation toolkit*, *Nucl. Instrum. Meth. A* **506** (2003) 250.
- [27] E. Barberio and Z. Was, *PHOTOS: A Universal Monte Carlo for QED radiative corrections*, *Comp. Phys. Commun.* **79**, 291 (1994).
- [28] T. Kuhr *et al.*, *The Belle II Core Software*, *Comput. Softw. Big Sci.* **3** (2019) 1.
- [29] “Belle II Analysis Software Framework (basf2), <https://doi.org/10.5281/zenodo.5574115>.”
- [30] M. Gelb *et al.*, *B2BII: Data Conversion from Belle to Belle II*, *Comput. Softw. Big Sci.* **2** (2018) 9.
- [31] F. Abudinen *et al.*, BELLE II collaboration, *Study of  $B \rightarrow D^*h$  decays using  $62.8 \text{ fb}^{-1}$  of Belle II data*, [[arXiv:2104.03628](https://arxiv.org/abs/2104.03628)].
- [32] H. Nakano *et al.*, *Search for new physics by a time-dependent CP violation analysis of the decay  $B \rightarrow K_S^0 \eta \gamma$  using the Belle detector*, Ph.D Thesis, Tohoku University (2014), unpublished. [[THESIS](https://arxiv.org/abs/1408.0001)].
- [33] H. Nakano *et al.*, *Measurement of time-dependent CP asymmetries in  $B^0 \rightarrow K_S^0 \eta \gamma$  decays*, *Phys. Rev. D* **97**, 092003 (2018).
- [34] G. C. Fox and S. Wolfram, *Observables for the Analysis of Event Shapes in  $e^+e^-$  Annihilation and Other Processes*, *Phys. Rev. Lett.* **41**, 1581 (1978).
- [35] S. H. Lee *et al.*, BELLE collaboration, *Evidence for  $B^0 \rightarrow \pi^0 \pi^0$* , *Phys. Rev. Lett.* **91**, 261801 (2003).
- [36] H. Kakuno *et al.*, BELLE collaboration, *Neutral B Flavor Tagging for the Measurement of Mixing-induced CP Violation at Belle*, *Nucl. Instrum. Meth. A* **533**, 516 (2004).
- [37] F. Abudinén *et al.*, *B-flavor tagging at Belle II*, *Eur. Phys. J. C* **82**, 283 (2022).
- [38] A. Hocker *et al.*, *TMVA- Toolkit for Multivariate Data Analysis*, [arXiv:physics/0703039](https://arxiv.org/abs/0703039).
- [39] H. Ikeda *et al.*, BELLE collaboration, *A detailed test of the CsI(Tl) calorimeter for BELLE with photon beams of energy between 20 MeV and 5.4 GeV*, *Nucl. Instrum. Meth. A* **441**, 401 (2000).
- [40] E. Nakano, *Belle PID*, *Nucl. Instrum. Meth. A* **494**, 402 (2002).
- [41] J. Charles *et al.*, CKMFITTER collaboration, *CP Violation and the CKM Matrix: Assessing the Impact of the Asymmetric B Factories*, *Eur. Phys. J. C* **41**, 1-131 (2005) [[online update](https://arxiv.org/abs/hep-ph/0412186)].
- [42] P. del Amo Sanchez *et al.*, BABAR collaboration, *Measurement of CP observables in  $B^\pm \rightarrow D_{CP} K^\pm$  decays and constraints on the CKM angle  $\gamma$* , *Phys. Rev. D* **82** 072004 (2010).

- [43] R. Aaji *et al.*, LHCb collaboration, *Measurement of CP observables in  $B^\pm \rightarrow D^* K^\pm$  and  $B^\pm \rightarrow D^* \pi^\pm$  decays using two-body D final states*, *J. High Energy Phys.* **81** (2021).